POLITECNICO
MILANO 1863

SCUOLA DI INGEGNERIA INDUSTRIALE
E DELL'INFORMAZIONE

EXECUTIVE SUMMARY OF THE THESIS

Coupling of membrane reactor and electrolyzer for green hydrogen production: carbon-neutral and carbon-negative solutions

TESI MAGISTRALE IN ENERGY ENGINEERING – INGEGNERIA ENERGETICA

AUTHOR: FRANCESCO LARDAIOLI

ADVISOR: Prof. MARCO BINOTTI

CO-ADVISORS: Ing. GIOELE DI MARCOBERARDINO, Ing. MICHELE ONGIS

ACADEMIC YEAR: 2021-2022

1. Introduction

In the decarbonizing challenge, hydrogen is a key player to achieve net zero emissions society, but, currently, less than 1% of H_2 production comes from renewable sources. Green hydrogen production deployment is thus necessary. One of the possible pathways is the exploitation of a carbon-neutral feed, such as biogas, especially for decentralized applications. Over the last years, some EU projects are proposing Membrane Reactors (MRs) as an interesting technology to produce and separate H_2 in the same unit, reducing space and equipment with respect to the conventional process. The fundamental advantage of MRs is circumventing the equilibrium condition limit of conventional processes, thus achieving the same performance of conventional reforming systems at milder condition. Hydrogen permeation happens through solution-diffusion mechanisms, and it is driven by H_2 partial pressure difference between retentate side (where reactions product stream flows) and permeate side (where hydrogen is separated). MRs can use either fixed-bed or fluidized-bed configurations, but the second one has several advantages: an important

reduction of internal heat and mass transfer limitation, minimum pressure drops and homogeneous temperature distribution. MRs are not a commercial-ready technology yet, thus further analyses to optimize their operation and to assess their coupling with other green technologies are necessary.

2. Methodology

The core of this work is an H_2 production plant from biogas through autothermal reforming (ATR) in a Fluidized Bed Membrane Reactor (FBMR) replacing air with pure oxygen as oxidizing agent. H_2 separation in MRs is driven by H_2 partial pressure difference between the two membrane sides; in a system where the fuel is characterized by a high inert content (typically CO_2 molar fraction of 40-50%), if pure O_2 is fed instead of air, N_2 at retentate side is avoided, thus increasing H_2 partial pressure difference, enhancing the driving force. Moreover, the off-gases mainly consist of CO_2 and water, so a simple CCS system can be included. Starting from the O_2-fed highest efficiency MR-based solution (found from O_2-air comparison), different layouts of an ATR-FBMR plant coupled with a Proton Exchange Membrane (PEM) electrolyzer to produce oxygen in situ and PV panels, have been techno-economically evaluated, considering both on-grid and off-grid solutions, described in Table 2.1. Conceptual scheme examples of complete on-grid coupling configuration and off-grid coupling configuration are provided in Figure 2.1.

Case name	Description
AIR CASE	On-grid benchmark case
PV-AIR CASE	On-grid benchmark case assisted by PV field
PEM-ATR	On-grid PEM-ATR plant
PV-PEM-ATR	On-grid PEM-ATR assisted by PV field
PV-BESS-PEM-ATR	On-grid PEM-ATR assisted by PV and battery (BESS)
OFF-GRID	Off-grid PEM-ATR plant with PV, BESS and O_2 tank

Table 2.1 - Configurations evaluated.

After water separation from off-gases, a rich-CO_2 stream is obtained and two CO_2 selling scenario have been evaluated: case A foresees CO_2 selling at ambient condition, while in case B CO_2 is injected into a pipeline, making the plant carbon-negative.

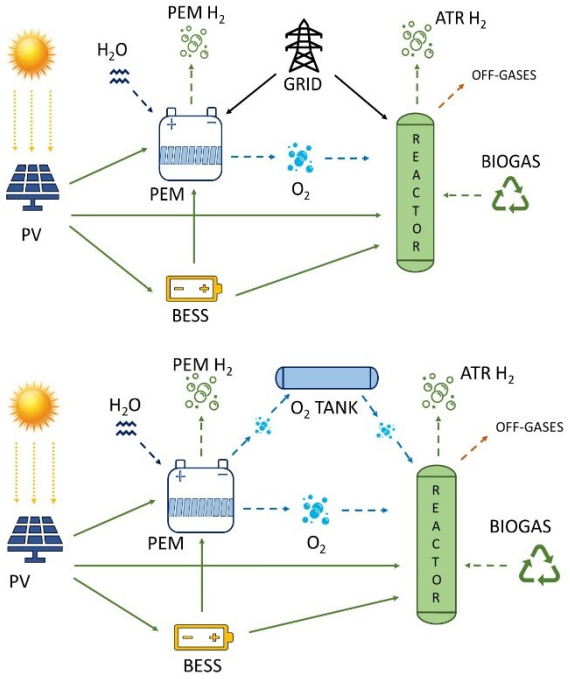

Figure 2.1 - Above: on-grid PV-BESS-PEM-ATR configuration. Below: off-grid configuration.

The ATR-FBMR plant, in Figure 2.2, is simulated in Aspen Plus [1], with an integrated Aspen Custom Modeler unit for the FBMR reactor. The Aspen flowsheet solve energy and mass balance of this section while the integration of the electrolyser, PV panels, BESS and the grid is developed with a specific VBA tool in Microsoft Excel to solve components control strategy, annual energy and mass balance and to optimize the components size.

First, a technical comparison with an air-fed case developed in MACBETH project [2], used as benchmark, is carried out. The comparison has been made varying membranes number considering the same target (H_2 production of 100 kg/day delivered at 20 bar), same biogas composition, same reactor temperature (500°C) and pressure (12 bar), same operative hours (7500 h/y). Hydrogen Recovery Factor (HRF), (Equation (2.1)) and system efficiency (η_{sys}), (Equation (2.2)) are the main KPIs to compare O_2 and air case [1]:

$$HRF = \frac{\dot{n}_{H_2,perm}}{4 \cdot (\dot{n}_{CH_4,in} - \dot{n}_{CH_4,ox})} \quad (2.1)$$

$$\eta_{sys} = \frac{\dot{m}_{H_2,perm} \cdot LHV_{H_2}}{\dot{m}_{BG,f} \cdot LHV_{BG} + \frac{W_{aux}}{\eta_{el,ref}}} \quad (2.2)$$

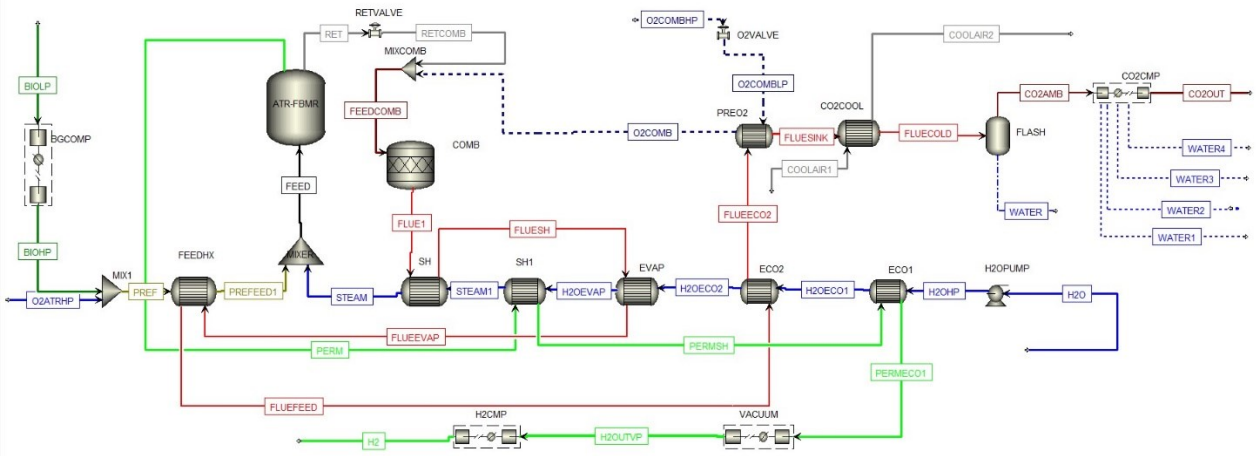

Figure 2.2 - ATR plant layout with O_2 (case B).

HRF is defined as the ratio between pure H_2 separated ($\dot{n}_{H_2,perm}$) and the maximum theoretical amount of hydrogen that can be produced if all CH_4 fed (excluding the amount burned) is converted according to reactions (R.3.1), (R.3.2), (R.3.3). System efficiency evaluates the energy output as H_2 produced, with respect to biogas and primary energy input. W_{aux} is the electricity of the plant auxiliaries, while $\eta_{el,ref}$ (45%) is the average electric efficiency of the power generating park [3].

Once the technical comparison is assessed, the coupling configurations are going to be compared with air-fed benchmark case. Levelized Cost Of Hydrogen (LCOH) (Equation (2.3) [3]) is used to compare the configurations. ATR-FBMR LCOH has been computed through CCF method as in [3], integrating coupling components through the cost model explained in [4].

$$LCOH = \frac{\sum TPC_c \cdot CCF_c + \sum C_{O\&M,c}}{kg_{H_2}} \qquad (2.3)$$

Hydrogen yearly productions have been evaluated through a hourly year-long simulation performed in Microsoft Excel, where electrolyzer model has been developed too. Solar radiation data (reference year is 2019) have been taken from PVgis tool, obtaining a yearly hourly profile of PV electricity generation in kWh/kW_P for Catania (Sicily). This procedure has been detailed in [4], where a coupling between PV and PEM has been performed.

3. Models

3.1 FBMR Model

Fluidized bed membrane reactor (FBMR) model simulates H_2 production and separation through MR, adopting Peng-Robinson equation of state and including methane steam reforming (R.3.1), water gas shift (R.3.2) and methane oxidation (R.3.3) reactions.

$$CH_4 + H_2O \leftrightarrow 3H_2 + CO \qquad (R.3.1)$$
$$CO + H_2O \leftrightarrow CO_2 + H_2 \qquad (R.3.2)$$
$$CH_4 + 2O_2 \rightarrow CO_2 + 2H_2O \qquad (R.3.3)$$

FBMR is a cylindrical vessel (coordinate z is the length) with membranes vertically placed from the top. Richardson Equation (3.4) describes H_2 permeation highlighting the relation between H_2 permeation flux per unit of area $J_{H_2,perm}(z)$ and H_2 partial pressure difference ($p^n_{H_2,ret}(z) - p^n_{H_2,perm}(z)$).

$$J_{H_2,perm}(z) = \frac{P^0_{H_2} \cdot exp\left(\frac{-E_{a,perm}}{RT}\right)}{t_{SL}} \cdot \left(p^n_{H_2,ret}(z) - p^n_{H_2,perm}(z)\right) \qquad (3.4)$$

Permeation model parameters, like activation energy of permeation process ($E_{a,perm}$), pre-exponential factor of membrane permeability $P^0_{H_2}$ and double-skin membranes features, like thickness of membrane selective layer t_{SL}, have been taken from [1]. In FBMR model are varied:

- Air/O_2 to ensure autothermal behaviour;
- H_2O to have Steam-Carbon-ratio equal to 3 at the beginning of membrane region;
- biogas to produce 100 kgH_2/day;

- reactor diameter to have gas superficial velocity and minimum fluidization velocity ratio (u_0/u_{mf}) equal to 1.5.

3.2 PEM Electrolyzer Model

Electrolyzer functioning is simulated through a modeled polarization curve ($i - V_{cell}$ curve). Each current density (i) and cell voltage (V_{cell}) couple, is an operating point, which provides the overall current (I), the overall voltage (ΔV), thus, the overall power (P) required, depending on cell area (A_{cell}) and on cell number (N_{cell}), as in Equations (3.5), (3.6), (3.7).

$$I = i \cdot A_{cell} \quad (3.5)$$
$$\Delta V = V_{cell} \cdot N_{cell} \quad (3.6)$$
$$P = I \cdot \Delta V \quad (3.7)$$

Polarization curve has been modeled starting from reversible cell voltage, computed through Nernst Equation and adding irreversible losses [5]:

- activation losses (modeled as in [5]);
- ohmic losses (modeled as in [6]);
- diffusion losses (modeled as in [6]);

The parameters to model the $i - V_{cell}$ curve have been reported in Table 3.1. The curve has been validated comparing temperature, pressure and exchange current density effects, with [7], [8].

Parameter	Value	Ref.
Membrane thickness δ_m	183 μm	[9]
Membrane H_2O activity a	1	[6]
Membrane hydration λ_m	$\lambda_m = f(a)$	[6]
Membrane conductivity σ_m	$\sigma_m = f(\lambda_m, T)$	[6]
Cathode and anode charge transfer coefficient	$\alpha_c = 0.5; \alpha_a = 2$	[5]
Cathode and anode exchange current density	$i_{0,cat} = 1 \cdot 10^{-1} \frac{A}{cm^2}$ $i_{0,an} = 2 \cdot 10^{-6} \frac{A}{cm^2}$	[7]

Table 3.1 - PEM model main parameters.

Faraday efficiency (modeled as in [10]) is used to pass from ideal to real H_2 and O_2 production.

$$\dot{n}_{H_2} = \frac{i}{2F} \cdot A_{cell} \cdot N_{cell} \cdot \eta_{Faraday} \quad (3.8)$$
$$\dot{n}_{O_2} = \frac{i}{4F} \cdot A_{cell} \cdot N_{cell} \cdot \eta_{Faraday} \quad (3.9)$$

According to equations (3.8) and (3.9), once that a certain production is required, depending on cell number and cell area, a current density i is detected. That i in $i - V_{cell}$ curve, allows to find the correspondent cell voltage (thus the required power). Applying this logic scheme in a reverse way, PEM production according to input power could be found. Relations to link these equations have been modeled, in order to easily pass from input power to PEM production or vice versa, once that cell area and cell number are defined.

3.3 PV, BESS, tank, CO_2 removal

The PV electricity generation profile, obtained by PVgis tool, considers the following aspects: shallow angle reflection, spectrum changes effect, hourly dependence on irradiance and module temperature, degradation with age and system losses [11]. "Aleo Solar Module P23" (nominal peak power of 325 W_p) [12] has been adopted, and land utilization has been computed assuming: no shadow at noon of 21st December, azimuth equal to -5° and slope of PV panel equal to 34° (values optimized by PVgis).

BESS (Li-ion) provides electricity avoiding grid withdrawal or allowing grid independence in off-grid case. In Table 3.2 the main parameters for BESS model are reported.

Parameter	Value	Ref.
Round-trip efficiency	95%	[13]
Maximum depth of discharge	90%	[14]

Table 3.2 - BESS model main parameters.

The oxygen tank is assumed to be kept at 15°C (ambient temperature) and it has been modeled through Ideal Gas Law (reduced temperature and reduced pressure around 1.9 and 0.6, respectively). Tank minimum pressure is set to be 13 bar, in order to properly feed ATR plant at 12 bar.

CCS system, after water separation, in scenario B, adopts a five-stage CO_2 compressor to bring rich-CO_2 stream (purity greater than 95%) at injection conditions (125 bar, 25°C) [15].

4. Economic assumptions and methodology

Economic analysis' aim is to compute overall plant LCOH. Plant lifetime is set to be 20 years, but PEM and BESS have lifetime of 10 years, thus replacement cost at year t of component c ($I_{replace,c,t}$) (Equation (4.1)) should be actualized using Weighted Average Capital Cost (WACC), as in [4].

$$I_{replace,act,c} = \sum_{t=1}^{Lifetime} \frac{I_{replace,c,t}}{(1+WACC)^t} \quad (4.1)$$

Actualized replacement cost is added to initial investment cost $I_{0,c}$ forming TPC_c (Equation (4.2)) for the component c.

$$TPC_c = I_{eq,c} = I_{0,c} + I_{replace,act,c} \quad (4.2)$$

The equivalent annual investment cost ($I_{eq,annual,c}$) is allocated as constant instalment along the plant lifetime, finding an annual share of the investment cost through Capital Charge Factor (CCF) [3].

$$I_{eq,annual,c} = TPC_c \cdot CCF_c + C_{O\&M,c} \quad (4.3)$$

The plant is composed by technologies with different readiness level, affecting investment valorisation. To avoid overpaying commercial technology, two WACCs, are assumed. For ATR it is assumed to be 13.1% (CCF of 16% [3]), while for the other technologies 8% (CCF of 9.24%) [4]. ATR plant cost are computed, like air-case, as in [3]. The costs assumed for the other technologies are detailed (exception for variable OPEX due to small relevance) in Table 4.1 and taken from [4],[16],[17]. According to the case evaluated two CO_2 selling price have been assumed: 35 €/tonCO_2 [18] for case A and 50 €/tonCO_2 [19] for case B. In off-grid, where PEM production is variable, an excess of O_2 could be generated and sold at 150 €/tonO_2 [20].

	$I_{0,c}$	Fix OPEX	$I_{replace,c,t}$
PEM	1000 €/kW	20 €/kW	400 €/kW
PV	831.5€/kW$_P$	13 €/kW$_P$	/
BESS	500 €/kWh	10 €/kWh	300€/kWh
Tank	1.23 k€/m^3	12.31€/m^3	/

Table 4.1 – Costs for the different technologies.

5. Results

The use of oxygen instead of air in the MACBETH system results in an higher HRF and in a reduction of membranes number. By increasing membranes number, the HRF is increased in both cases, reducing the biogas fed, thus improving system efficiency. However, by increasing membranes number two limits shall be considered. The first is that adjacent membrane cannot be closer than 2 cm, otherwise, loss in separation capability is experimentally detected [1]. The second concerns feed temperature: when HRF increases CH_4 content in retentate decreases, thus retentate LHV is reduced, providing a colder feed to FBMR, reducing its performance [1]. Minimum distance limit is reached adopting 122 and 147 membranes for O_2-case and air-case, respectively, providing the best performance. Comparison of technical features in air and oxygen most performant cases are reported in Table 5.1.

Parameter	Air-case	O_2-case
Membranes number	147	122
Reactor Diameter [m]	0.47	0.43
Biogas [kmol/h]	1.30	1.24
Air/O_2 FBMR [kmol/h]	1.27	0.25
Air/O_2 burner [kmol/h]	1.88	0.15
T feed [°C]	437.3	473.6

Table 5.1 - Air and O_2 case comparison.

Performance results for air and O_2 case are reported in Table 5.2 and in Figure 5.1, where air-case without air-compression is reported because it is coherent with O_2-case, where O_2 is given at reactor condition. Even neglecting air compression, O_2 feed improves plant performance. Furthermore, LCOHs are decreasing at higher membranes number, because purchasing biogas, which input is reducing, is a relevant share (around 40%) of equivalent annual cost.

	HRF	η_{sys}	W_{aux} [kW]
O_2	71.39%	65.42%	22.93
Air	68.29%	60.25%	27.84
Air (no CMP)	68.29%	63.01%	23.30

Table 5.2 – Results of air and oxygen comparison.

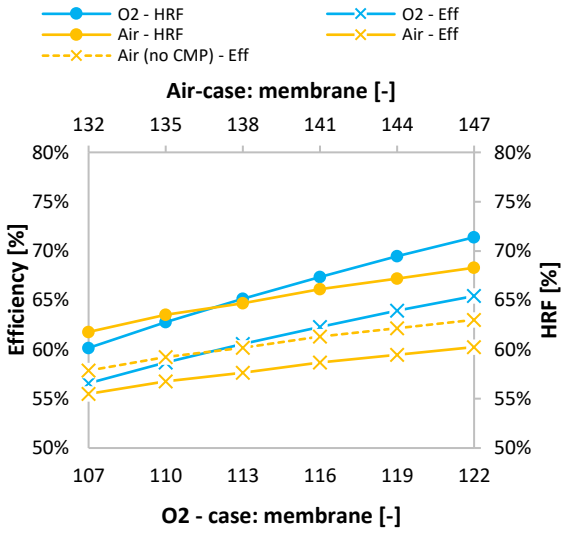

Figure 5.1 - Efficiency and HRF comparison.

Since performance improvement is detected, techno-economic convenience of oxygen-fed ATR plant coupled with a PEM electrolyzer have been evaluated in different configurations, sharing the O_2-case features (detailed in Table 5.1 and Table 5.2) which maximizes the ATR plant performance.

The first coupling is set up with PEM-ATR plant powered by the grid. PEM produces exactly the oxygen needed by ATR (0.40 kmolO_2/h) for 7500 h/y, working at constant load, at 60°C and at 21 bar, thus H_2 from PEM could be mixed with H_2 from ATR. The results of on-grid PEM-ATR configurations are detailed in Table 5.3. Since air-case LCOH is equal to 4.96 €/kgH_2, these solutions are not economically convenient.

Parameter	Case A	Case B
PEM size [kW]	96.7	
PEM i [A/cm²]	1.28	
PEM V_{cell} [V]	1.84	
PEM consumption [kW]	89	
ATR consumption [kW]	22.93	
CO_2 compressor [kW]	/	7.20
ATR [kgH_2/day]	100	
PEM [kgH_2/day]	39.2	
Plant efficiency	47.15%	45.38%
LCOH (no CO_2) [€/kgH_2]	5.48	
LCOH [€/kgH_2]	5.17	5.21

Table 5.3 - On-grid PEM-ATR features.

Two air-case break-even scenarios have been developed. Firstly, CO_2 selling price has been investigated, while the second is concerning PEM technology cost. It has been demonstrated that 60 €/tonCO_2 and 78.5 €/tonCO_2 are break-even CO_2 selling prices for case A and case B, respectively. Concerning PEM technology cost, even considering 2030 forecasting, break-even is not reached. This is due to the small share (only 6%) of PEM technology in plant equivalent annual cost, against 33% of electricity purchasing cost.

In order to supply cheaper electricity, a PV field, with LCOE equal to 56.5 €/MWh (lower than electricity purchasing price hypothesis equal to 120 €/MWh), is assumed to be installed. PV sizes which minimizes LCOH of on-grid PEM-ATR plant assisted by PV field are reported in Table 5.4, while PEM features are the same as in Table 5.3. Electricity surplus revenues is not a driver for PV size choice, otherwise, being LCOE lower than electricity selling price assumed (60 €/MWh), PV size would skyrocket.

Air-case could be fed by PV field too, this reduces its LCOH from 4.96 €/kgH_2 to 4.83 €/kgH_2. Results of LCOHs when plants are assisted by PV field are shown in Table 5.4.

Parameter	Air case	Case A	Case B
PEM size [kW]	/	96.7	96.7
PV size [kW_P]	48.8	180	195
$\frac{PV_{power}}{PEM_{power}}$	/	1.86	2.02
LCOH [€/kgH_2]	4.86	4.89	4.92
LCOH (PV rev) [€/kgH_2]	4.83	4.82	4.86

Table 5.4 - On-grid plants assisted by PV field.

BESS introduction in PV-PEM-ATR plant is worsening the economic performance, thus further details are not going to be reported.

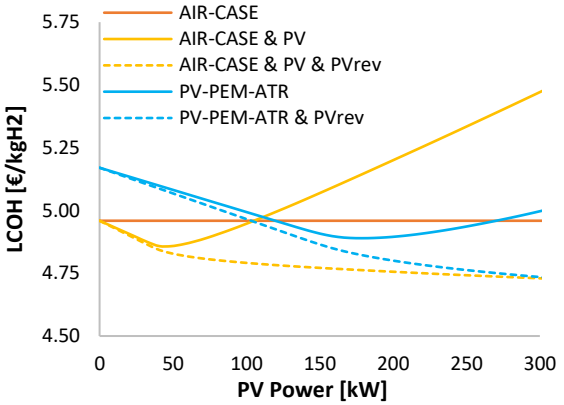

Figure 5.2 - LCOH comparison with air and oxygen-best-case (Case A).

Parameter	Case A	Case B
PEM size [kW]	258	215
PV size [kW_P]	812.5	812.5
BESS size [kWh]	800	900
Tank size [kgO_2]	300	300
ATR operative hours [h/y]	7756	7775
LCOH (no selling) [€/kgH_2]	5.82	6.13
LCOH cut by CO_2 sold [€/kgH_2]	-0.29	-0.43
LCOH cut by O_2 sold [€/kgH_2]	-0.11	-0.06
LCOH [€/kgH_2]	5.42	5.64

Table 5.5 - Off-grid sizes and resulting LCOH.

Due to the relevance of electricity purchasing cost a sensitivity analysis on its price has been performed. It is proved that 120 €/MWh is

practically a break-even price; with lower values, hydrogen from O_2-fed ATR plant is cheaper.

Off-grid components sizes are larger than on-grid ones, thus greater LCOHs are expected. However, since PEM production (set at 60°C and at 30 bar to charge the tank) is variable, depending on input power, incomes are provided by O_2-selling too. Being off-grid, the ATR plant operative hours are not bound to be 7500 h/y as in on-grid cases. This affects streams flow rate and, thus, incomes from CO_2 , from O_2, and LCOHs (values reported in Table 5.5) are affected too.

A summary of results of components size and LCOHs for the set-up which minimize LCOHs for each configuration, divided by CO_2 treatment and selling, is reported in Table 5.6.

Case name	PEM [kW]		PV [kW_P]		BESS [kWh]		O_2 tank [kg]		LCOH [€/kgH_2]		LCOH - PV revenues [€/kgH_2]	
AIR CASE	/		/		/		/		4.96		/	
PV-AIR CASE	/		48.8		/		/		4.86		4.83	
	Case A	Case B	Case A	Case B	Case A	Case B	Case A	Case B	Case A	Case B	Case A	Case B
PEM-ATR	96.7		/		/		/		5.17	5.21	/	
PV-PEM-ATR	96.7		180	195	/		/		4.89	4.92	4.82	4.86
PV-BESS-PEM-ATR	96.7		195	211	50		/		4.94	4.97	4.86	4.88
OFF-GRID	258	215	812.5	812.5	800	900	300		5.42	5.64	/	

Table 5.6 - Results of the best configurations for each configurations if CO_2 is sold at ambient condition (Case A) or if CO_2 is injected into pipeline (Case B).

6. Conclusions

It has been quantified that feeding oxygen, instead of air, for an ATR plant assisted by FBMR is beneficial, increasing HRF (of around 3 percentage point) and the system efficiency (from 63.01% to 65.42%). Furthermore, the number of membranes adopted is reduced, from 147 of air case to 122 of O_2-case.

Techno-economic convenience of coupling ATR fed by oxygen and PEM electrolyzer has been demonstrated, reaching LCOH practically equivalent to benchmark air-case, whether the plant is assisted by PV field. A note could be done concerning off-grid case, where the electricity used is 100% renewable, providing a completely green hydrogen solution, useful especially for those applications which require H_2 and O_2 production in situ. Particularly interesting are carbon-negative configurations, where the environmental benefits of carbon-negative solution are coupled with economic results close to air-case.

References

[1] M. Ongis, G. Di Marcoberardino, M. Baiguini, F. Gallucci, and M. Binotti, "Optimization of small-scale hydrogen production with membrane reactors," pp. 1–26, 2023.

[2] "EU project MACBETH." https://www.macbeth-project.eu/.

[3] G. Di Marcoberardino, S. Foresti, M. Binotti, and G. Manzolini, "Potentiality of a biogas membrane reformer for decentralized hydrogen production," *Chem. Eng. Process. - Process Intensif.*, vol. 129, no. August 2017, pp. 131–141, 2018, doi:

10.1016/j.cep.2018.04.023.

[4] E. Crespi, P. Colbertaldo, G. Guandalini, and S. Campanari, "Design of hybrid power-to-power systems for continuous clean PV-based energy supply," *Int. J. Hydrogen Energy*, vol. 46, no. 26, pp. 13691–13708, 2021, doi: 10.1016/j.ijhydene.2020.09.152.

[5] M. Carmo, D. L. Fritz, J. Mergel, and D. Stolten, "A comprehensive review on PEM water electrolysis," *Int. J. Hydrogen Energy*, vol. 38, no. 12, pp. 4901–4934, 2013, doi: 10.1016/j.ijhydene.2013.01.151.

[6] E. W. Saeed and E. G. Warkozek, "Modeling and Analysis of Renewable PEM Fuel Cell System," *Energy Procedia*, vol. 74, pp. 87–101, 2015, doi: 10.1016/j.egypro.2015.07.527.

[7] B. Han, S. M. Steen, J. Mo, and F. Y. Zhang, "Electrochemical performance modeling of a proton exchange membrane electrolyzer cell for hydrogen energy," *Int. J. Hydrogen Energy*, vol. 40, no. 22, pp. 7006–7016, 2015, doi: 10.1016/j.ijhydene.2015.03.164.

[8] V. Liso, G. Savoia, S. S. Araya, G. Cinti, and S. K. Kær, "Modelling and experimental analysis of a polymer electrolyte membrane water electrolysis cell at different operating temperatures," *Energies*, vol. 11, no. 12, 2018, doi: 10.3390/en11123273.

[9] R. Hancke, T. Holm, and Ø. Ulleberg, "The case for high-pressure PEM water electrolysis," *Energy Convers. Manag.*, vol. 261, no. December 2021, 2022, doi: 10.1016/j.enconman.2022.115642.

[10] B. Yodwong, D. Guilbert, M. Phattanasak, W. Kaewmanee, M. Hinaje, and G. Vitale, "Faraday's efficiency modeling of a proton exchange membrane electrolyzer based on experimental data," *Energies*, vol. 13, no. 18, pp. 1–14, 2020, doi: 10.3390/en13184792.

[11] EU Science Hub, "PVgis tool." https://re.jrc.ec.europa.eu/pvg_tools/en/.

[12] "Aleo Solar Module P23." https://www.aleo-solar.com/app/uploads/sites/6/2016/02/P23_320-325W_EN_web.pdf.

[13] T. Feehally, A. J. Forsyth, R. Todd, S. Liu, and N. K. Noyanbayev, "Efficiency Analysis of a High Power Grid-connected Battery Energy Storage System," *IET Int. Conf. Power Electron. Mach. Drives*, pp. 1–6, 2018.

[14] Y. Liu, Y. G. Liao, and M. C. Lai, "Effects of Depth-of-Discharge, Ambient Temperature, and Aging on the Internal Resistance of Lithium-Ion Battery Cell," *Int. Conf. Electr. Comput. Energy Technol. ICECET 2021*, no. December, pp. 9–10, 2021, doi: 10.1109/ICECET52533.2021.9698495.

[15] S. P. Peletiri, N. Rahmanian, and I. M. Mujtaba, "CO2 Pipeline design: A review," *Energies*, vol. 11, no. 9, 2018, doi: 10.3390/en11092184.

[16] S. Giuliano, M. Puppe, and K. Noureldin, "Power-to-heat in CSP systems for capacity expansion," *AIP Conf. Proc.*, vol. 2126, no. July, 2019, doi: 10.1063/1.5117589.

[17] T. Mayer, M. Semmel, M. A. Guerrero Morales, K. M. Schmidt, A. Bauer, and J. Wind, "Techno-economic evaluation of hydrogen refueling stations with liquid or gaseous stored hydrogen," *Int. J. Hydrogen Energy*, vol. 44, no. 47, pp. 25809–25833, 2019, doi: 10.1016/j.ijhydene.2019.08.051.

[18] J. Kim, C. A. Henao, J. E. Miller, and E. Stechel, "Methanol production from CO2 using solar-thermal energy: process development and techno-economic analysis," no. September, 2011, doi: 10.1039/C1EE01311D.

[19] A. Bhardwaj, C. McCormick, and J. Friedmann, "Opportunities and limits of CO2 utilization pathways: Techno-economics, critical infrastructure needs, and policy priorities," *Abstr. Pap. 262nd ACS Natl. Meet. Expo. Atlanta, GA, United States, August 22-26, 2021*, no. May, 2021.

[20] D. Bellotti, A. Sorce, M. Rivarolo, and L. Magistri, "Techno-economic analysis for the integration of a power to fuel system with a CCS coal power plant," *J. CO2 Util.*, vol. 33, no. March, pp. 262–272, 2019, doi: 10.1016/j.jcou.2019.05.019.